Influence of different starting models on near-surface two-dimensional full waveform inversion

Influence de différents modèles initial sur près de la surface inversion bidimensionnelle de forme d'onde complète

Joseph P. Vantassel
Civil, Architectural, and Environmental Engineering, The University of Texas at Austin, USA, jvantassel@utexas.edu

Brady R. Cox
Civil and Environmental Engineering, Utah State University, USA

ABSTRACT: All aspects of geotechnical engineering require an understanding of the composition and distribution of subsurface properties. Yet, as a field of study, geotechnical engineering lags behind other disciplines with similar imaging needs. This lag is due in part to the challenging nature of 2D/3D subsurface imaging, as well as a historical over-reliance on 1D subsurface approximations. Recently, however, several stress-wave methods have achieved increased use for 2D/3D near-surface characterization, one of the most promising of which is full waveform inversion (FWI). However, FWI, as with all inverse problems, suffers from non-uniqueness, which results in multiple solutions that may appear quite different to rank as equivalent in terms of the inverse problem's objective function. Or in other words, multiple different potential solutions often fit the experimental data equally well, resulting in uncertainty as to which is most representative of the subsurface. This paper examines uncertainty in the 2D FWI inverse problem by considering how different starting models affect the accuracy of the solution. In particular, this paper considers the effect of different inversion starting models on the solution of a classic geotechnical problem; characterization of a site composed of soil over undulating bedrock. Three different categories of starting model are considered: those with constant stiffness, those with linearly increasing stiffness with depth, and those derived from other 1D/2D seismic methods (i.e., surface-wave analysis).

RÉSUMÉ : Tous les aspects de l'ingénierie géotechnique nécessitent une compréhension de la composition et de la distribution des propriétés souterraines. Pourtant, en tant que domaine d'étude, l'ingénierie géotechnique est à la traîne par rapport aux autres disciplines ayant des besoins d'imagerie similaires. Ce retard est en partie dû à la nature difficile de l'imagerie souterraine 2D/3D, ainsi qu'à une sur-dépendance historique sur les approximations souterraines 1D. Récemment, cependant, plusieurs méthodes d'onde de contrainte ont atteint une utilisation accrue pour la caractérisation 2D/3D près de la surface, l'une des plus prometteuses étant l'inversion complète de la forme d'onde (FWI). Cependant, FWI, comme pour tous les problèmes inverses, souffre de la non-unicité, ce qui entraîne des solutions multiples qui peuvent sembler assez variables pour se classer comme équivalentes en termes de fonction objectif du problème inverse. En d'autres termes, plusieurs solutions potentielles différentes correspondent souvent aussi bien aux données expérimentales, ce qui entraîne une incertitude quant à savoir laquelle est la plus représentative du sous-sol. Cet article examine l'incertitude dans le problème inverse FWI 2D en considérant comment différents modèles de départ affectent la précision de la solution. En particulier, cet article considère l'effet de différents modèles de départ d'inversion sur la solution d'un problème géotechnique classique; caractérisation d'un site composé de sol sur substrat rocheux ondulé. Trois catégories différentes de modèles de départ sont considérées: ceux avec une rigidité constante, ceux avec une rigidité croissante linéairement avec la profondeur, et ceux dérivés d'autres méthodes sismiques 1D/2D (c'est-à-dire l'analyse des ondes de surface).

KEYWORDS: full waveform inversion, starting model, surface waves, MASW.

1 INTRODUCTION

Full waveform inversion (FWI) is a data-fitting procedure whereby a synthetic seismic wavefield, generated by numerically solving the associated wave equations, is matched to an experimental seismic wavefield, acquired through field experiments (Tarantola, 1984). The matching process involves iteratively modifying an assumed starting model through which the synthetic waveforms propagate until the synthetic and experimental wavefields are in acceptable agreement, as determined by a wavefield objective/misfit function. Once the iterative optimization process is complete, the final modified model is considered to be an accurate representation of the subsurface.

FWI can be understood to be composed of two components: (1) a forward problem, which can propagate the seismic wavefield input(s) [i.e., source(s)] through an assumed model to the desired wavefield output location(s) [i.e., receiver location(s)] so that the seismic wavefield misfit can be calculated, and (2) an optimization technique, which can minimize the seismic wavefield misfit by generating improved subsurface models. For the former, there are various numerical techniques available to solve the associated wave equations with sufficient accuracy (e.g., spectral element, finite element), making the selection of any particular method of secondary concern. In contrast, the optimization technique employed is of paramount importance, as its ability to converge to the true solution is not guaranteed (Nocedal and Wright, 2006). Optimization techniques can be broadly grouped into two main categories: global and local. Global optimization methods are generally more rigorous than local optimization methods, as they search a large number of potential models in a broad, predefined parameter space, but as a result are more computationally expensive. Despite their computational expense, a few researchers have used global optimization methods for FWI (Tran and Hiltunen, 2012; Sajeva et al., 2016; Datta and Sen, 2016; Mojica and Kukreja, 2019), however, their use remains relatively unpopular. In their place, local optimization methods are used. Local optimization methods minimize the objective

function by refining an initial/starting model provided by the user. By searching in the vicinity of a user-specified starting model, local optimization methods are able to converge to a solution faster than global optimization methods, however, because of their limited scope, local optimization methods are more likely to become trapped in local minima and fail to converge to the global minima (i.e., the true solution). To limit the potential for local methods to become trapped in local minima, the starting model provided by the user should reside close to the true subsurface model.

Selecting an acceptable starting model for FWI is non-trivial, as at best its fitness may not be apparent until after attempting the time-consuming inversion process, and at worst its appropriateness (or, inappropriateness) may not ever be known. Various approaches have been proposed in the literature for developing initial starting models. These include simple heuristic approaches, such as assuming a constant velocity models or a model whose velocity increases linearly with depth (Tran and McVay, 2012; Kallivokas et al., 2013; Tran et al., 2019), and more complex approaches that use information derived from other techniques to find an approximate starting model, such as refraction, first-arrival travel-time tomography, surface wave methods, and migration velocity analysis (Weibull et al., 2012; Groos et al., 2017; Köhn et al., 2019; Pan et al., 2019; Wang et al., 2019). Importantly, the effectiveness of these approaches are rarely compared to one another in practice due to the computational cost of FWI. To emphasize how limited the literature is in this area, the only paper the authors could find on comparing different starting models was in regard to the specific use of teleseismic events (i.e., very distant earthquakes) for crustal scale (depths greater than 5 km) FWI (Beller et al., 2018). As the reader might suspect, the findings of the aforementioned work have very little (if any) applicability to the present study on near-surface characterization. In response, this paper seeks to understand the effects different starting models can have on the subsurface model recovered from FWI using a local optimization method.

2 COMPARISON OF DIFFERENT STARTING MODELS

To study the effect of using different starting models for FWI, this paper inverts waveforms from a single synthetic model using three types of starting models commonly used in the literature. The synthetic model used in this study is representative of a classic geotechnical problem; characterization of soil over undulating rock. The model is shown in terms of its shear wave velocity (Vs) in Figure 1. While the model presented in this paper is synthetic, the authors believe it is more realistic (and therefore more challenging for FWI) than models which are typically used in synthetic studies for several specific reasons. First, the soil's Vs increases with depth following an approximate relationship between Vs and mean effective stress for dense sand (Menq, 2003). Second, the interface between soil and rock is highly irregular, representing a challenging but reasonable subsurface condition. Third, and finally, the model includes moderately sized (~1-2 m in the vertical and ~4-6 m in the horizontal directions) stiff and soft regions in the soil and rock applied using a laterally correlated Gaussian random field to approximate the reality of a heterogeneous subsurface. To completely define the elastic properties of the synthetic model, compression wave velocity (Vp) and mass density were developed by assuming simple relationships between Vs and the parameter of interest. In particular, the Vp model assumed unsaturated conditions with a Poisson's ratio of 0.33 for the soil (i.e., Vs < 300 m/s) and 0.2 for rock-like material (i.e., Vs > 360 m/s). For intermediate materials, the Poisson's ratio was linearly interpolated. The mass

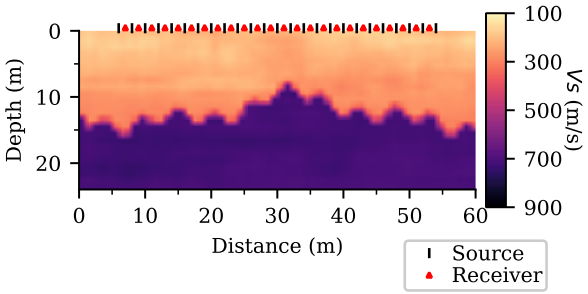

Figure 1. The synthetic subsurface model, presented in terms of its shear wave velocity (Vs), to be recovered using full waveform inversion (FWI) using different starting models. The synthetic model's Vs is consistent with a site composed of dense sand over undulating rock.

density model assumed a value of 2100 kg/m^3 for rock-like material and 2000 kg/m^3 elsewhere.

Experimental waveforms for the synthetic model were generated by solving the P-SV elastic forward problem using finite difference with a staggered-grid discretization (Virieux, 1986), as implemented in the open-source software DENISE (Köhn, 2011; Köhn et al., 2012). The top of the model followed the free-surface boundary condition (Levander, 1988), whereas the sides and bottom were truncated using perfectly matched layers (Komatitsch and Martin, 2007). Waveforms were generated for a typical 2D FWI experimental setup consisting of 24 receivers (spaced at 2 m) and 25 source locations (1 m off both ends and between each receiver spacing). The positions of the sources and receivers are shown in Figure 1. All source locations utilized the same source wavelet consisting of a 15 Hz high-cut filtered spike, which was used to simulate a sledgehammer impact. The numerical simulation utilized a 5E-5 second time step for a duration of 1 second. The simulation used a 6th order finite difference operator in space and a 2nd order finite difference operator in time. To ensure the simulation's numerical stability, all models used a 0.2-m pixel.

The three different starting models considered in this study are: constant, linear, and one derived from 1D/2D seismic methods. The constant starting model's Vs, shown in Figure 2a, was selected by finding the constant value with a minimum square difference between it and the true Vs model over the top 10 m (i.e., the predominantly soil-like portion of the model). While this approach cannot be employed in practice, as the true Vs model is unknown, it was done here in this synthetic study to give the constant starting model the most likely chance of success and to avoid the time-consuming process of attempting different constant starting models, as is typically required in practice. The linear starting model's Vs, presented in Figure 2c, was defined in a similar manner as the constant starting model, however, the least-square-difference computation was not restricted to the model's upper 10 m. Rather, the Vs of the staring model was allowed to vary linearly with depth in order to achieve the minimum least-square-difference relative to the entire true model's Vs. The starting model derived from other 1D/2D methods was developed using the multi-channel analysis of surface waves (MASW) method (Park et al., 1999). The MASW starting model's Vs, presented in Figure 2e, was created by first simulating seismic wavefields using two additional source locations (located at 5 m off either end of the array). The dispersion data obtained from processing the seismic wavefields obtained from all source locations outside of the array were inverted using 3 different Layering by Number (LN) parameterizations, following the recommendations of Vantassel and Cox (2021a). The 100 lowest misfit Vs profiles from each of the three different LN parameterizations were then statistically

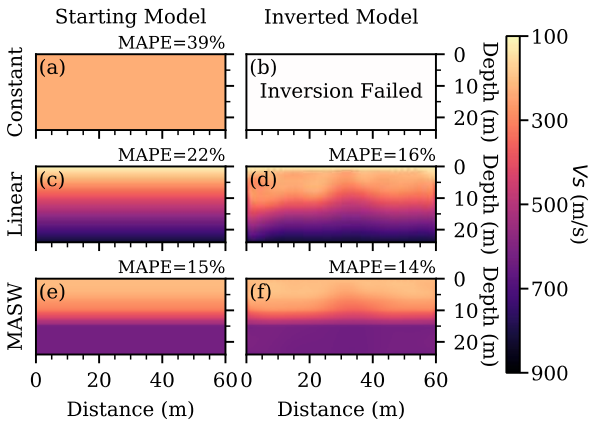

Figure 2. Comparison of three different starting models used to initiate full waveform inversion (FWI) as a means to attempt to recover the true synthetic subsurface model shown in Figure 1. Panels (a), (c), and (e) show the constant, linear, and multichannel analysis of surface waves (MASW) starting models, adjacent to their inverted models after FWI (i.e., panels (b), (d), and (f), respectively) in terms of their Vs. The mean absolute percent error (MAPE) of each FWI Vs model relative to the true Vs model is shown in the upper right of each panel. Note that no inverted model is available for the constant starting model, panel (b), as the inversion failed.

combined into a single, discretized median 1D Vs profile, which was extended over the entire width of the domain. To develop the necessary Vp and mass density values to completely define the starting model, the same simple rules discussed with respect to the development of the synthetic model were applied.

The same FWI settings and multi-scale inversion workflow were used for each of the three starting models. FWI was performed using the same open-source software DENISE (Köhn, 2011; Köhn et al., 2012) as was used for the forward problem described above. This allows FWI to have the best chance of success, as the experimental/synthetic target waveforms and the theoretical waveforms are computed using the same implementation of the forward problem. The gradient was preconditioned using the Limited-Memory Broyden-Fletcher-Goldfarb-Shanno (LBFGS) technique (Byrd et al., 1995) where it was allowed to retain 10 prior updates. To reduce large gradients at the model's source locations, circular preconditioning tapers with a radius of 1 m were applied around each source location. To still permit the model to update in these locations during the inversion, the 25 sources were simulated separately and the preconditioning only applied to the currently active source. To limit the introduction of spurious small-scale features, the model gradient was smoothed using a 2D Gaussian stencil extending over a 1 m by 1 m area (i.e., recall for solving the forward problem a 0.2-m pixel size was deemed necessary for stability). The optimal step length was selected using a line search. Inversions utilized a multi-scale workflow (Bunks et al., 1995) to mitigate the potential for cycle skipping and to improve convergence. The multi-scale inversion workflow used three stages with overlapping frequency ranges of 0 - 7 Hz, 0 - 13 Hz, and full signal. Each stage was required to consist of at least 10 optimization iterations and was allowed to conclude after either the change in the misfit function became less than 1% or 100 iterations were performed. The only exception to these rules is if a simulation became unstable in the middle of the stage without yet reaching one of the aforementioned stopping criteria. If this occurred, the inversion was restarted in the subsequent stage. During the inversion process, all three model variables (Vs, Vp, and mass density) were allowed to be updated to ensure no penalty was applied to models which started further from the true solution and which, therefore, likely contained worse estimates of Vp and mass density. As the wavefield is not strongly sensitive to mass density (Köhn et al., 2012), the gradient when applying the mass density update was scaled by a factor of ½ to discourage the creation of artifacts in the density model related to large updates early in the inversion process.

The results of FWI for the three starting models are presented in panels (b), (d), and (f) of Figure 2. Beginning with the inversion of the constant starting model, unfortunately, no results are available, as the model failed during the first iteration of the multi-scale inversion workflow. Numerous attempts were made to tweak the inversion's settings, however, ultimately no result was able to be obtained. Potential causes for the failure of the constant Vs starting model is discussed later after presenting the results from the other two starting models. The FWI results obtained from the linear starting model in terms of Vs, shown in Figure 2d, indicate increased Vs in the 0-5 m depth range (with the notable exception of the upper 1 m), decreased Vs in the 5-10 m depth range, and minimal changes throughout the remainder of the model (10-24 m depth range). Furthermore, the inverted Vs model also contains a vague indication of the concave-down shape of the bedrock interface beginning near the center of the Vs model, however, the location and velocities of the 2D soil-to-bedrock interface are poorly resolved. The FWI results obtained from the MASW starting model in terms of Vs, shown in Figure 2f, indicate only minimal changes in Vs relative to the starting model. The only change of note is a slight increase of Vs at the model's center. To quantify the goodness of fit of each FWI-derived model to the true model, the mean absolute percent error (MAPE) (i.e., the mean of the absolute value of the difference between the predicted and true Vs normalized by the true Vs) is presented in the upper right of each panel of Figure 2. A comparison of the MAPE for the three starting models (left column) reveals that for this example, the MASW starting model was the best (i.e., lowest MAPE), whereas the constant starting model was the worst (i.e., largest MAPE). This is, of course, despite the efforts described previously to ensure the constant and linear starting models were the closest possible approximation of the true model. It is believed that the relatively large MAPE of the constant starting model is responsible, at least in part, for the failure of the constant starting model to produce FWI results. The large MAPE indicates the constant model is an inadequate approximation of the true model, and therefore, beyond the reach of the local optimization algorithm. It is important to highlight that the MASW model outperformed the constant and linear starting models in terms of its MAPE both before and after FWI. This is somewhat surprising considering that the procedure for developing the constant and linear models used here cannot be performed in practice, as it requires knowledge of the true subsurface model, whereas the MASW approach can be performed in practice. Comparing the MAPE of the linear and MASW starting model's, both before and after inversion, echoes the conclusions made previously that the linear model updated more significantly (i.e., MAPE decreases from 22% to 16% following FWI) than the MASW model, which remained largely unchanged (i.e., MAPE only decreased from 15% to 14%). The cause of these different update behaviors is discussed next in context of the seismic waveforms.

While a quantitative metric, such as MAPE, can be quite useful for comparing velocity models it is also important to make comparisons qualitatively. A qualitative comparison between the linear and MASW starting model FWI results (Figure 2d and 2f, respectively) hints that to some the linear starting model may have perform slightly better (i.e., the opposite conclusion as obtained following MAPE) as it gives a more meaningful

indication of the variability of the bedrock interface. We note this, because the FWI results from the linear and MASW starting models indicate two competing approximations of the true model. If FWI was performed using only the linear starting model, the rock interface would be perceived to be variable (which is true) with a gradual velocity contrast between the soil and rock (which is false). In contrast, if only the MASW model was used, the rock interface would be perceived to be essentially flat (which is false) with a strong velocity contrast between the soil and rock (which is true). Depending on the perspective of the viewer, one may be considered a better approximation of the true model. For example if a realistic estimate of the rock's variability is the primary concern, the linear starting model could be considered superior, whereas if a realistic estimate of the soil and rock velocity contrast is the primary concern, the MASW starting model could be considered superior. Ultimately, neither exactly matches the true model, thereby highlighting the need for caution when interpreting FWI results when the issue of non-uniqueness has not been rigorously investigated. We note here that while the use of two starting models allowed for some approximate understanding of the non-uniqueness of the FWI problem it is almost certainly not rigorous enough and it is therefore still likely underestimating the phenomena. Therefore, we emphasize that additional work is required to develop approaches to improve convergence to the true solution regardless of starting model and quantify any residual effects of non-uniqueness in FWI to aid in model interpretation.

Figure 3 compares the waveforms associated with the three starting models before and after FWI with those from the true subsurface model. The waveforms are compared for the source located at a distance of 30 m (i.e., at the center of the model). A qualitative comparison of the waveforms from the three starting models (i.e., the first column in Figure 3) reveals that the MASW starting model matches the true waveforms better than the other two approaches (i.e., constant and linear), with the initial body wave and later surface wave arrivals being well captured at all offsets. As a quantitative measure, the mean square error (MSE) between the true waveforms and the starting model/inverted waveforms are presented in the upper right of each panel. Note we use MSE as the error metric here to be consistent with the objective function of the FWI algorithm used in this study. Interestingly, the MSE of the waveforms are inconsistent with the MAPE of the starting models presented previously (recall Figure 2). It was expected that the constant starting model, which had the highest MAPE (MAPE=39%), would also have the highest waveform MSE. Instead, the linear starting model, not the constant starting model, has the highest waveform MSE. The mismatch between Vs model error and waveform error indicates that while the linear starting model's waveforms are the worst match to the true model's waveforms, it is a better approximation of the true model (MAPE=22%) than the constant starting model. The fact that the MSE waveform misfit may not always be indicative of the goodness of the associated subsurface model is the result of the non-uniqueness of the FWI problem and a major cause for concern when performing FWI. Certainly, additional work is required to investigate the non-uniqueness present in FWI and the relationship between an inverted model's similarity to the true model and that of the similarity of its waveforms to that of the true model's waveforms. Returning to the issue of the failed inversion of the constant starting model, a qualitative assessment of its waveforms reveals that they poorly approximate the true waveforms, with nearly an entire cycle being missed at the furthest receiver offsets. It is believed that these missing/skipped cycles, which are known to be a side effect of the inadequacy of the starting model and especially problematic for FWI (Shah et al., 2012), are the primary cause of the constant model's failure to produce inversion results.

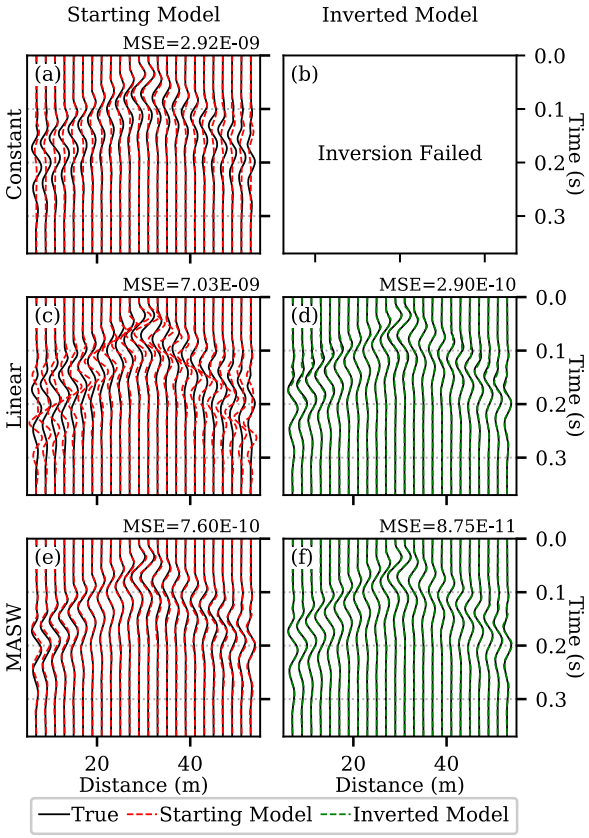

Figure 3. Qualitative comparison between synthetic waveforms before (panels (a), (c), and (e)) and after (panels (b), (d), and (f)) FWI with the waveforms obtained from the true model for the source located at a distance of 30 m (i.e., at the center of the model). The mean square error (MSE) of the various waveforms is shown in the upper right of each panel. Note that no waveforms are available after inversion for the constant starting model, panel (b), as the inversion failed.

When comparing the successful FWI results, the waveforms from the linear and MASW starting models following FWI are shown to well capture those from the true model (see Figure 3d and 3f, respectively). The fact that the linear model's waveforms are in relatively poor agreement with those from the true model prior to FWI (Figure 3c) and the MASW model's waveforms are in relatively good agreement with those from the true model prior to FWI (Figure 3e) explains the observations made previously in regard to Figure 2. Namely, that the linear model was updated rather significantly during FWI in order to achieve a better match to the waveforms, whereas the MASW model was updated only minimally during FWI because, as Figure 3 illustrates, the MASW model prior to FWI was already able to produce waveforms that matched the majority of true model's waveforms. Therefore, for the MASW model, significant refinement by the optimization algorithm was unnecessary. Yet, despite the good agreement ultimately achieved between the waveforms of the linear and MASW inverted models and those of the true model (Figure 3d and 3f), comparisons between the actual inverted linear and MASW Vs models (Figure 2d and 2f) with the true Vs model (Figure 1) reveals that neither closely resembles the true subsurface model. This serves to highlight the effect of non-uniqueness in FWI, and draw attention to the need for future studies to propose strategies to mitigate and/or quantify non-uniqueness in FWI. Mitigation strategies may include the ability to incorporate a priori information, such as from common invasive geotechnical testing, into the inverse problem to limit

the solution's multiplicity (Tarantola, 2005). Whereas, quantification strategies will allow the rigorous quantification of uncertainty and non-uniqueness in the inverse problem for the most general case where no a priori information is available. Note that such a technique for quantifying uncertainty and non-uniqueness has recently been proposed by the authors for the one-dimensional surface wave inversion problem (Vantassel and Cox, 2021b).

3 CONCLUSIONS

This paper performs 2D FWI for a single, synthetic subsurface model using three different categories of commonly used starting models: constant, linear, and MASW. Results show that the selected starting model can have a significant effect on the resulting inverted model, with the inverted models generally not changing significantly relative to the starting model, despite the inverted model's waveforms matching the true model's waveforms quite well. Due to the significant influence of the starting model in FWI, it is recommend that the use of any starting model be considered carefully. General recommendations to consider when selecting a FWI starting model include selecting only those models that: (1) are believed to be a reasonable approximation to the subsurface, and (2) have pre-FWI waveforms which are a good approximation of the experimental waveforms. A relatively simple approach for producing model's which follow these recommendations is by using existing surface-based methods for developing 1D/2D starting models, for example the MASW method was used in this study. However, we also note that while the waveforms of the inverted model may match the experimental waveforms quite well, as in the case of the linear and MASW models presented in this study, this agreement does not necessarily guarantee that the recovered model will closely match the true subsurface model due to the inverse problem's non-uniqueness. This study highlights that future work is required to better understand, mitigate, and quantify non-uniqueness in FWI.

4 ACKNOWLEDGEMENTS

The forward solution and full waveform inversion (FWI) algorithm used in this study are from v1.3 of the open-source software DENISE (Köhn, 2011; Köhn et al., 2012). The computations in this work were performed on the Texas Advanced Computing Center's (TACC's) cluster Stampede2 using an allocation provided through the DesignSafe-CI (Rathje et al., 2017). The multi-channel analysis of surface wave (MASW) data was processed using v0.1.0b0 of the open-source Python package, *swprocess* (Vantassel, 2021). Surface wave inversion was performed using v2.10.1 of the Dinver module (Wathelet et al., 2004) of the open-source software Geopsy (Wathelet et al., 2020) with pre- and post-processing facilitated by v0.3.1 of the open-source Python package, *swprepost* (Vantassel, 2020). The figures in this paper were created using Matplotlib v3.1.2 (Hunter, 2007). This work was supported by the U.S. National Science Foundation grant CMMI-1931162. However, any opinions, findings, and conclusions or recommendations expressed in this material are those of the authors and do not necessarily reflect the views of the National Science Foundation.

5 REFERENCES

Beller, S., Monteiller, V., Combe, L., Operto, S., Nolet, G., 2018. On the sensitivity of teleseismic full-waveform inversion to earth parametrization, initial model and acquisition design. Geophysical Journal International 212, 1344–1368. https://doi.org/10.1093/gji/ggx480

Bunks, C., Saleck, F.M., Zaleski, S., Chavent, G., 1995. Multiscale seismic waveform inversion. Geophysics 60, 1457–1473. https://doi.org/10.1190/1.1443880

Byrd, R.H., Lu, P., Nocedal, J., Zhu, C., 1995. A Limited Memory Algorithm for Bound Constrained Optimization. SIAM journal on scientific computing 16, 1190–1208.

Datta, D., Sen, M.K., 2016. Estimating a starting model for full-waveform inversion using a global optimization method. GEOPHYSICS 81, R211–R223. https://doi.org/10.1190/geo2015-0339.1

Groos, L., Schäfer, M., Forbriger, T., Bohlen, T., 2017. Application of a complete workflow for 2D elastic full-waveform inversion to recorded shallow-seismic Rayleigh waves. GEOPHYSICS 82, R109–R117. https://doi.org/10.1190/geo2016-0284.1

Hunter, J.D., 2007. Matplotlib: A 2D Graphics Environment. Computing in Science Engineering 9, 90–95. https://doi.org/10.1109/MCSE.2007.55

Kallivokas, L.F., Fathi, A., Kucukcoban, S., Stokoe, K.H., Bielak, J., Ghattas, O., 2013. Site characterization using full waveform inversion. Soil Dynamics and Earthquake Engineering 47, 62–82. https://doi.org/10.1016/j.soildyn.2012.12.012

Köhn, D., 2011. Time domain 2D elastic full waveform tomography (Ph. D.). Kiel University, Kiel, Germany.

Köhn, D., De Nil, D., Kurzmann, A., Przebindowska, A., Bohlen, T., 2012. On the influence of model parametrization in elastic full waveform tomography. Geophysical Journal International 191, 325–345. https://doi.org/10.1111/j.1365-246X.2012.05633.x

Köhn, D., Wilken, D., De Nil, D., Wunderlich, T., Rabbel, W., Werther, L., Schmidt, J., Zielhofer, C., Linzen, S., 2019. Comparison of time-domain SH waveform inversion strategies based on sequential low and bandpass filtered data for improved resolution in near-surface prospecting. Journal of Applied Geophysics 160, 69–83. https://doi.org/10.1016/j.jappgeo.2018.11.001

Komatitsch, D., Martin, R., 2007. An unsplit convolutional perfectly matched layer improved at grazing incidence for the seismic wave equation. GEOPHYSICS 72, SM155–SM167. https://doi.org/10.1190/1.2757586

Levander, A.R., 1988. Fourth-order finite-difference P-SV seismograms. Geophysics 53, 1425–1436. https://doi.org/10.1190/1.1442422

Menq, F.-Y., 2003. Dynamic Properties of Sandy and Gravelly Soils. The University of Texas at Austin, Austin, Texas.

Mojica, O.F., Kukreja, N., 2019. Towards automatically building starting models for full-waveform inversion using global optimization methods: A PSO approach via DEAP + Devito. arXiv:1905.12795 [physics].

Nocedal, J., Wright, S.J., 2006. Numerical optimization, 2nd ed. ed, Springer series in operations research. Springer, New York.

Pan, Y., Gao, L., Bohlen, T., 2019. High-Resolution Characterization of Near-Surface Structures by Surface-Wave Inversions: From Dispersion Curve to Full Waveform. Surv Geophys 40, 167–195. https://doi.org/10.1007/s10712-019-09508-0

Park, C.B., Miller, R.D., Xia, J., 1999. Multichannel analysis of surface waves. GEOPHYSICS 64, 800–808. https://doi.org/10.1190/1.1444590

Rathje, E.M., Dawson, C., Padgett, J.E., Pinelli, J.-P., Stanzione, D., Adair, A., Arduino, P., Brandenberg, S.J., Cockerill, T., Dey, C., Esteva, M., Haan, F.L., Hanlon, M., Kareem, A., Lowes, L., Mock, S., Mosqueda, G., 2017. DesignSafe: New Cyberinfrastructure for Natural Hazards Engineering. Nat. Hazards Rev. 18, 06017001. https://doi.org/10.1061/(ASCE)NH.1527-6996.0000246

Sajeva, A., Aleardi, M., Stucchi, E., Bienati, N., Mazzotti, A., 2016. Estimation of acoustic macro models using a genetic full-waveform inversion: Applications to the Marmousi model. GEOPHYSICS 81, R173–R184. https://doi.org/10.1190/geo2015-0198.1

Shah, N., Warner, M., Nangoo, T., Umpleby, A., Stekl, I., Morgan, J., Guasch, L., 2012. Quality assured full-waveform inversion: Ensuring starting model adequacy, in: SEG Technical

Program Expanded Abstracts 2012. Presented at the SEG Technical Program Expanded Abstracts 2012, Society of Exploration Geophysicists, pp. 1–5. https://doi.org/10.1190/segam2012-1228.1

Tarantola, A., 2005. Inverse problem theory and methods for model parameter estimation. Society for Industrial and Applied Mathematics.

Tarantola, A., 1984. Inversion of seismic reflection data in the acoustic approximation. GEOPHYSICS 49, 1259–1266. https://doi.org/10.1190/1.1441754

Tran, K.T., Hiltunen, D.R., 2012. Two-Dimensional Inversion of Full Waveforms Using Simulated Annealing. J. Geotech. Geoenviron. Eng. 138, 1075–1090. https://doi.org/10.1061/(ASCE)GT.1943-5606.0000685

Tran, K.T., Jalinoos, F., Agrawal, A.K., 2019. Characterization of Concrete Pile Groups with 2-D Seismic Waveform Tomography. J Nondestruct Eval 38, 25. https://doi.org/10.1007/s10921-019-0565-x

Tran, K.T., McVay, M., 2012. Site characterization using Gauss–Newton inversion of 2-D full seismic waveform in the time domain. Soil Dynamics and Earthquake Engineering 43, 16–24. https://doi.org/10.1016/j.soildyn.2012.07.004

Vantassel, J., 2021. jpvantassel/swprocess: v0.1.0b0. Zenodo. https://doi.org/10.5281/zenodo.4584129

Vantassel, J., 2020. jpvantassel/swprepost: v0.3.1. Zenodo. https://doi.org/10.5281/zenodo.3901859

Vantassel, J.P., Cox, B.R., 2021a. SWinvert: a workflow for performing rigorous 1-D surface wave inversions. Geophysical Journal International 224, 1141–1156. https://doi.org/10.1093/gji/ggaa426

Vantassel, J.P., Cox, B.R., 2021b. A procedure for developing uncertainty-consistent Vs profiles from inversion of surface wave dispersion data. Soil Dynamics and Earthquake Engineering 145, 106622. https://doi.org/10.1016/j.soildyn.2021.106622

Virieux, J., 1986. P-SV wave propagation in heterogeneous media: Velocity-stress finite-difference method. Geophysics 51, 13.

Wang, Y., Miller, R.D., Peterie, S.L., Sloan, S.D., Moran, M.L., Cudney, H.H., Smith, J.A., Borisov, D., Modrak, R., Tromp, J., 2019. Tunnel detection at Yuma Proving Ground, Arizona, USA — Part 1: 2D full-waveform inversion experiment. GEOPHYSICS 84, B95–B105. https://doi.org/10.1190/geo2018-0598.1

Wathelet, M., Chatelain, J.-L., Cornou, C., Giulio, G.D., Guillier, B., Ohrnberger, M., Savvaidis, A., 2020. Geopsy: A User-Friendly Open-Source Tool Set for Ambient Vibration Processing. Seismological Research Letters. https://doi.org/10.1785/0220190360

Wathelet, M., Jongmans, D., Ohrnberger, M., 2004. Surface-wave inversion using a direct search algorithm and its application to ambient vibration measurements. Near Surface Geophysics 2, 211–221. https://doi.org/10.3997/1873-0604.2004018

Weibull, W., Arntsen, B., Nilsen, E., 2012. Initial velocity models for Full Waveform Inversion, in: SEG Technical Program Expanded Abstracts 2012. Presented at the SEG Technical Program Expanded Abstracts 2012, Society of Exploration Geophysicists, pp. 1–4. https://doi.org/10.1190/segam2012-1025.1